Corrosion Science 77 (2013) 342–349

Contents lists available at ScienceDirect

Corrosion Science

journal homepage: www.elsevier.com/locate/corsci

New zinc–rare earth alloys: Influence of intermetallic compounds on the corrosion resistance

Delphine Veys-Renaux [a,*], Khadoudj Guessoum [a,b], Emmanuel Rocca [a], Nicolas David [a], Kamel Belhamel [b]

[a] Institut Jean Lamour-UMR CNRS 7198, Université de Lorraine-CNRS, BP 70239, Vandoeuvre-lès-Nancy 54506, France
[b] Laboratoire des Matériaux Organiques, Département de Génie des Procédés, Faculté de Technologie, Université de Béjaia, Béjaia 06000, Algeria

ARTICLE INFO

Article history:
Received 7 March 2013
Accepted 29 August 2013
Available online 6 September 2013

Keywords:
A. Zinc
A. Rare earth elements
A. Intermetallics
C. Thermodynamic diagrams
B. SEM
B. Polarization

ABSTRACT

New ZnRE 1–2 wt.% alloys (RE = Ce, La and Mischmetal) were synthesized. Microstructural analyses reveal that rare-earth metals are exclusively present in intermetallic phases contained within the zinc matrix: $CeZn_{11}$ or $LaZn_{13}$ in binary alloys; $Ce_{1-x}La_xZn_{11}$ and $Ce_yLa_{1-y}Zn_{13}$ in Zn–Mischmetal alloys. This phase equilibrium is confirmed by a thermodynamic description of the Zn-rich corner of Zn–Ce–La system. Both intermetallic phases $CeZn_{11}$ and $LaZn_{13}$ induce a cathodic inhibition of the corrosion of the Zn–RE alloys in comparison with pure zinc. In the specific case of cerium addition, a significant anodic inhibition is also observed.

1. Introduction

In the field of cathodic protection of steel structures exposed to atmospheric and marine media, zinc is extensively used. Actually, compared to other metals with low redox potentials (like aluminum and magnesium), zinc is electrochemically active in a wide range of media but keep a relatively low dissolution rate, so that the life-time of the sacrificial anode in zinc or coating is satisfactory in many environments [1]. Nevertheless, the addition of alloying elements, besides the improvement of workability, is necessary to enhance the mechanical properties and the corrosion resistance of zinc in practice [2]. Indeed, the natural corrosion layer on zinc, named "white rust", is generally composed of voluminous, lamellar and not well adherent products as hydrozincite $Zn_5(CO_3)_2(OH)_6$, zinc hydroxysulfate $Zn_4SO_4(OH)_6{\cdot}4H_2O$, zinc hydroxychloride $Zn_5(OH)_8Cl_2{\cdot}H_2O$ [3,4], that are poorly protective.

In the case of nickel, cobalt or manganese addition to zinc, the improvement of corrosion protection is generally attributed to a selective dissolution leading to a surface enrichment in alloying element, which reduces the rate of white rust formation [5,6]. In case of aluminum addition, the corrosion of alloys induces the formation of a double lamellar hydroxide, namely $Zn_6Al_2CO_3(OH)_{16}{\cdot}4H_2O$, that inhibits the growth of crumbly white rust [7] .

Further addition of small amounts of rare-earth elements to ZnAl 5 wt.% alloy improves its corrosion resistance through the formation of a "lanthanide-doped" corrosion products layer according to Rosalbino's studies [8,9]. In these alloys the rare earth seems to be present in ternary intermetallic phases according to their analysis. Recently, an electrochemical study of Zn–Ce alloys in corrosive medium has shown that an optimum concentration of cerium, around 2 wt.%, is necessary to reach a optimum in corrosion resistance [10].

In all cases, the change in the chemical composition or in the growth rate of the corrosion products induce a modification of the morphology of the corrosion layer and an improvement of its adhesion, which lead to a decrease of the corrosion rate compared to the pure zinc.

On the other hand, many studies point out that the effect of alloying elements is also very dependent on their distribution in the alloy, and especially the distribution of the different intermetallic phases containing the alloying element [11–13].

The purpose of this work is thus to study the possibility to reinforce the natural corrosion products of zinc by alloying zinc with cerium, lanthanum and mischmetal (Ce/La: 75/25 wt.%). New zinc–cerium, zinc–lanthanum and zinc–lanthanum–cerium alloys were synthesized until 2 wt.% in rare-earth elements. The microstructure of the alloys, analyzed by scanning electron microscopy (SEM), electron micro-probe analysis (EPMA) and X-ray diffraction (XRD), is compared to the thermodynamic data of the phase diagrams. In the case of Zn-La-Ce system, a modeling of the Zn-rich corner is proposed in this paper.

Then, the effect of rare earth elements on the corrosion behavior of the alloys was investigated in aerated corrosive reference water

* Corresponding author. Tel.: +33 3 83 68 46 30.
E-mail address: delphine.veys-renaux@univ-lorraine.fr (D. Veys-Renaux).

0010-938X/$ - see front matter © 2013 Elsevier Ltd. All rights reserved.
http://dx.doi.org/10.1016/j.corsci.2013.08.024

(simulating wet/dry cycles under environmental exposure) by using different stationary electrochemical methods. In order to understand the electrochemical relation between the intermetallic phases and the zinc matrix and to highlight the specificities of these new alloys, pure intermetallic phases synthesized as bulk material were also studied.

2. Experimental details

2.1. Synthesis and characterization of alloys and pure intermetallic phases

ZnRE 1–2 wt.% alloys (RE = Ce, La and Mischmetal: Ce 75 wt.%/La 25 wt.%) as well as RE-enriched pure intermetallic phases ($CeZn_{11}$ and $LaZn_{13}$) investigated in this work were synthesised from cerium pieces (99.999 wt.% nominal purity), lanthanum pieces (99.9999 wt.% nominal purity), mischmetal pieces (Ce 75 wt.%–La 25 wt.%) and pure zinc (99.9999 wt.% nominal purity), supplied by Alfa Aesar. Rare earth metals were cut and abraded under oil and washed with n-hexane. The alloys and pure intermetallic phases were prepared into closed alumina crucibles (Al_2O_3), using a vertical Pyrox furnace maintained at 600 °C during 24 h under pure argon flux, to prevent oxidation of metals and volatilization of zinc. Then, the ingots of alloys were re-melted in a muffle furnace at 550 °C for 20 min under a nitrogen atmosphere, to be rapidly cast in plates in an aluminum mold (60 × 60 × 3 mm) under atmospheric conditions. After synthesis, the samples were analyzed by X-ray diffraction with a classical diffractometer (X'Pert Pro/Philips), using Cu $K\alpha_1$ wavelength (λ_1 = 1.54051 nm) in Bragg–Brentano geometry. Microstructures of zinc alloys were investigated by backscattered scanning electron microscopy (SEM: Philips XL30) and analyzed by electron probe micro-analysis (micro-probe: CAMECA SX100). Each elemental analysis by EPMA is the average of ten different analysis points.

2.2. Thermodynamic calculations

The zinc corner of Ce–La–Zn diagram was modeled from the thermodynamic data of binary diagrams of literature. The Ce–Zn and La–Zn systems were respectively optimized by Wang et al. [14] and Qi et al. [15] according to the CALPHAD method [16]. According to several previous works [17,18], an optimized phase diagram for Ce–La system was calculated in this work and is presented in Fig 1a. The optimized coefficients obtained for Ce–La system are reported in Table 1.

In the Ce–La–Zn system, liquid, body-centered cubic (BCC A2), face-centered cubic (FCC A1), hexagonal close-packed (HCP A3) and double hexagonal close-packed (DHCP) are described with the substitutional solution model with excess terms described by the Redlich–Kister polynomials. Disordered substitutional solutions are represented by only one sublattice where all the atoms mix together. Concerning $CeZn_2$, $CeZn_5$, $CeZn_{11}$, Ce_2Zn_{17} and Ce_3Zn_{22} stoichiometric compounds and regarding the similarities of their respective crystallographic data with their respective opposite in the La–Zn border ($LaZn_2$, $LaZn_5$, $LaZn_{11}$, La_2Zn_{17} and La_3Zn_{22}), they are described as ternary solution phases with substitution of Ce by La at Zn ratio constant and treated as the formula $(Ce,La)_aZn_b$. All other intermediate compounds are modeled as stoichiometric compounds, namely CeZn, $CeZn_3$, Ce_3Zn_{11}, $Ce_{13}Zn_{58}$, $LaZn_4$, $LaZn_{13}$. The Gibbs energies of the pure elements, referred to the enthalpy of each element in its so-called standard element reference (SER) state (the stable state at 10^5 Pa and 298.15 K) were taken from the SGTE Pure Element (unary) Database [19].

The calculated Zn-rich corner of the Ce–La–Zn phases diagram is presented in Fig. 1b and the obtained set of parameters is summarized in Table 1.

2.3. Electrochemical characterisations

Electrochemical characterisations were carried out both on ZnRE alloys and on the pure $CeZn_{11}$ and $LaZn_{13}$ intermetallic phases after mechanical abrading on SiC paper up to grade 4000 and mirror-like polishing with 1 μm diamond paste. All the electrochemical experiments were performed in a reference corrosive solution (D 1384-87 ASTM standard water [20]: Na_2SO_4, 148 mg/l; $NaHCO_3$, 138 mg/l; NaCl, 165 mg/l (pH = 8.3; σ = 650 μS cm^{-1})), noted "ASTM water" in the text, whose composition simulates corrosion under environmental exposure [21,22]. The solution was

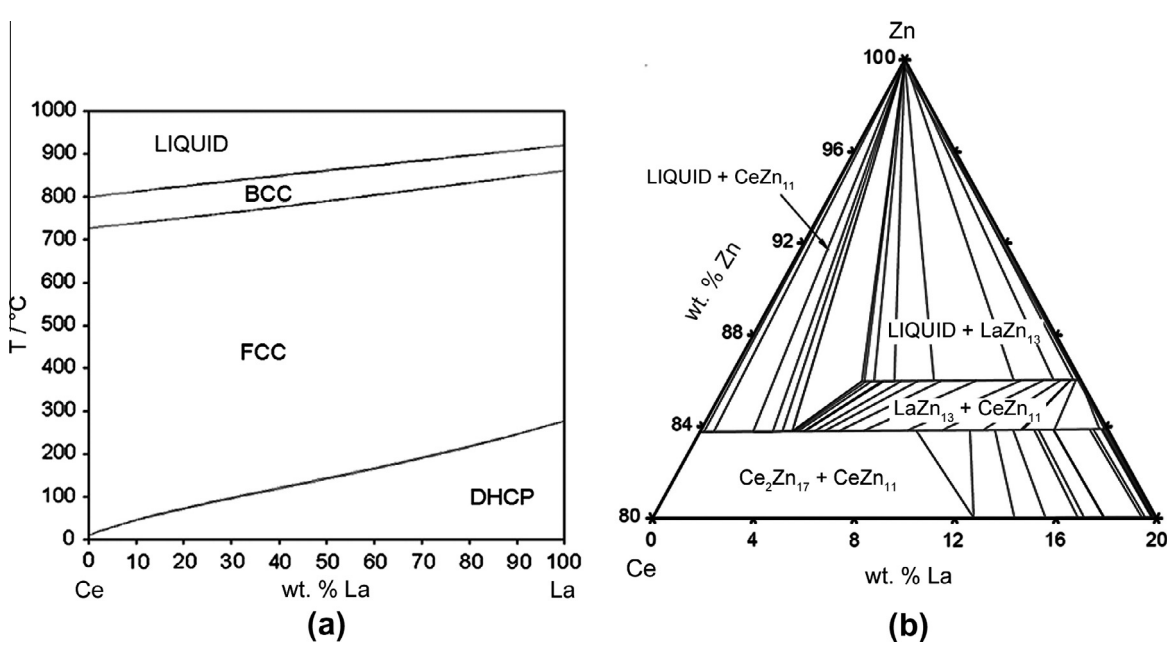

Fig. 1. Calculated phase diagram of Ce–La with optimized set of parameters based on experimental data [17,18] (a); Calculated ternary equilibria in the Zn-rich corner of the Ce–La–Zn phase diagram at 873 K based on experimental points from this work (b).

Table 1
Optimized Gibbs energy coefficients of the Ce–La–Zn system.

Phase	Model	Parameter	Coefficients a
Liquid	(Ce,La,Zn)	${}^{0}L^{L}_{Ce,La}$	+696.0015
		${}^{1}L^{L}_{Ce,La}$	+2172.273
$(Ce,La)Zn_{11}$	$(Ce,La)_1(Zn)_{11}$	${}^{0}L^{MZn_{11}}_{Ce,La:Zn}$	−556.436
$LaZn_{13}$	$(Ce,La)_1(Zn)_{13}$	$\Delta^{o}_{f}G^{LaZn_{13}}_{Ce:Zn}$	−16718.687
		${}^{0}L^{LaZn_{13}}_{Ce,La:Zn}$	+116.589

aerated by bubbling industrial air. The circular working electrode surface (3.14 cm^2) was horizontal, facing to a platinum grid used as counter electrode; the reference electrode was a KCl-saturated calomel electrode (SCE). Electrochemical tests were carried out at room temperature (20 °C ± 3 °C) using a Gamry instruments Framework (600 Potentiostat/Frequency Response Analyzer).

The following experimental sequence was used both on alloys and intermetallic bulk phases:

(a) Measurement of the corrosion potential (E_{corr}) during 24 h in ASTM corrosive water,
(b) Measurement of the anodic and cathodic polarization curves independently after 24 h immersion in ASTM water with a scan rate of 1 mV s^{-1} [23]. These curves were not ohmic-drop compensated. Nevertheless, the distance between the reference electrode and the working one was kept constant (1 cm) thanks to fixed positions in the electrochemical cell.

On the other hand, galvanic coupling measurements were performed in ASTM water between pure zinc and bulk intermetallic phases $CeZn_{11}$ and $LaZn_{13}$ (surface ratio 1/1).

2.4. Surface analysis after long-time immersion

To investigate the morphology and the chemical composition of the corrosion products, the alloys were immersed during 30 days in ASTM corrosive water and then observed in cross-section by backscattered scanning electron microscopy (FEG-SEM Jeol J7600F). Wave-length dispersive X-ray spectrometry (WDS Oxford Wave) was used to characterize the presence and repartition of the different elements in the corrosion layer.

Table 2
Compositions of intermetallic phases besides Zn matrix within ZnRE alloys.

Alloys	ZnCe	ZnLa	ZnMisch	
Intermetallic phases	$CeZn_{11}$	$LaZn_{13}$	$Ce_{1-x}La_xZn_{11}$	$Ce_yLa_{1-y}Zn_{13}$
Zn (at.%)	91.8 ± 0.5	92.4 ± 0.5	91.6 ± 0.5	92.4 ± 0.5
Ce (at.%)	8.2 ± 0.1	–	6.4 ± 0.1	4.8 ± 0.1
La (at.%)	–	7.3 ± 0.1	1.9 ± 0.1	2.6 ± 0.1

3. Results

3.1. Microstructural characterization of the synthesised alloys

SEM micrographs (Fig. 2) show a homogeneous dispersion of intermetallic precipitates (bright) within a zinc matrix (dark) for ZnCe, ZnLa as well as ZnMisch alloys. The solubility of cerium and lanthanum in this zinc matrix is close to zero, below the detection limit of these elements by EPMA measurements (Det. Lim. ≈ 600 ppm for Ce and La in ZnRE alloys). For each type of alloy, the compositions of intermetallic precipitates, resulting from EPMA measurements, are gathered in Table 2. Whatever the composition of the binary alloys, the composition of the intermetallic phases corresponds to the richest zinc containing intermetallic phases: $CeZn_{11}$ in the case of ZnCe alloys, $LaZn_{13}$ in the case of ZnLa alloys, in accordance with the binary diagrams [14,15]. These results are confirmed by the comparison between the diffractogramms of the alloys and the diffractogramms of $CeZn_{11}$ and $LaZn_{13}$ pure intermetallic phases, synthesized as bulk materials (Fig. 3a and 3b).

Concerning the ZnMisch 2 wt.% alloy, two populations of intermetallic phases are detected by EPMA analysis, corresponding to the $Ce_{1-x}La_xZn_{11}$ (with $x = 0.23$) and $Ce_yLa_{1-y}Zn_{13}$ (with y = 0.68)

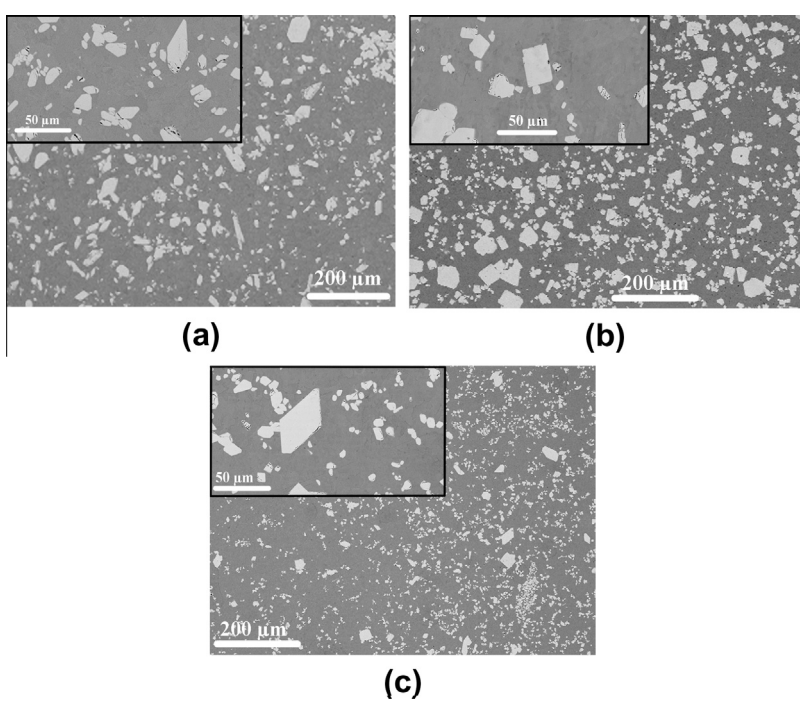

Fig. 2. Metallographic cross-sections of ZnRE alloys (SEM images): ZnCe 2 wt.% (a); ZnLa 2 wt.% (b); ZnMisch 2 wt.% (c).

composition. In this alloy, the quantities of each intermetallic phase are not sufficient to be detected by macroscopic XRD. Nevertheless, a more concentrated ZnMisch 15 wt.% was synthesized, and the diffractogram of this sample confirms the presence of the two crystallographic structures, $CeZn_{11}$ and $LaZn_{13}$, as displayed in the Fig. 3c. So, two kinds of intermetallic phases are in equilibrium in the Zn–La–Ce ternary system.

From thermodynamic data described in the experimental section, the thermodynamic simulation of the zinc-rich corner of the ternary system corroborates the possibility of equilibrium between the zinc matrix, $Ce_{1-x}La_xZn_{11}$ and $Ce_yLa_{1-y}Zn_{13}$ phases (Fig. 1). Some other experimental points would certainly be necessary to precise the solubility limit of cerium in $LaZn_{13}$.

The relatively high size of the intermetallic particules (until 50–100 μm in some areas) indicates that they are formed via a primary precipitation phenomenon in the zinc liquid phase (at 600 °C) because of their high melting point temperature (between 700 and 800 °C), which favors the growth of large and coarse intermetallic particles.

3.2. Electrochemical behavio of the alloys

The electrochemical behavior of the different synthesized alloys was investigated in ASTM water by recording the corrosion potentials during 24 h, then by performing separately cathodic and anodic potentiodynamic experiments. The results are compared with those obtained on pure zinc on Fig. 4.

Open-circuit potential values are confined in the range −1.1 V/SCE to −0.9 V/SCE whatever the immersion duration and the amount and nature of the addition elements. In all cases (pure zinc and alloys), the potential decreases during the four first hours, which corresponds to the dissolution of the original passive layer. Then, the open-circuit potential remains constant on pure zinc surface, whereas the addition of low quantities of rare-earth elements leads to a slight ennoblement, characterized by a gradual increase of the potential. This is the sign of a chemical modification of the corrosion products layer in the presence of rare earth alloying elements, enhancing the passivity of the alloys compared to pure zinc.

Consistently with open-circuit potential measurements, the potentiodynamic curves show a nobler corrosion potential for rare-earth metal containing alloys than for pure zinc. The first part of the cathodic curve (cathodic "plateau" between E_{corr} and −1.22 V/SCE), corresponding to O_2 reduction, is greatly affected by the addition of rare-earth elements: in comparison with pure zinc, the kinetic of O_2 reduction is divided by a factor ten in the case of ZnCe and ZnMisch alloys and by a factor hundred for ZnLa alloys. Below −1.22 V/SCE, the current density, mainly due to water reduction, is reduced to a lesser extent for lanthanum containing alloys. Regarding the anodic curve, only ZnCe alloys induce a modification of the electrochemical behavior with the appearance of a passivation plateau until -0.8 V/SCE. On this plateau, the anodic current density reaches 10 μA cm^{-2}, reduced by thirty in comparison with pure zinc. In the case of ZnLa binary alloys, a slight anodic inhibition is also observed.

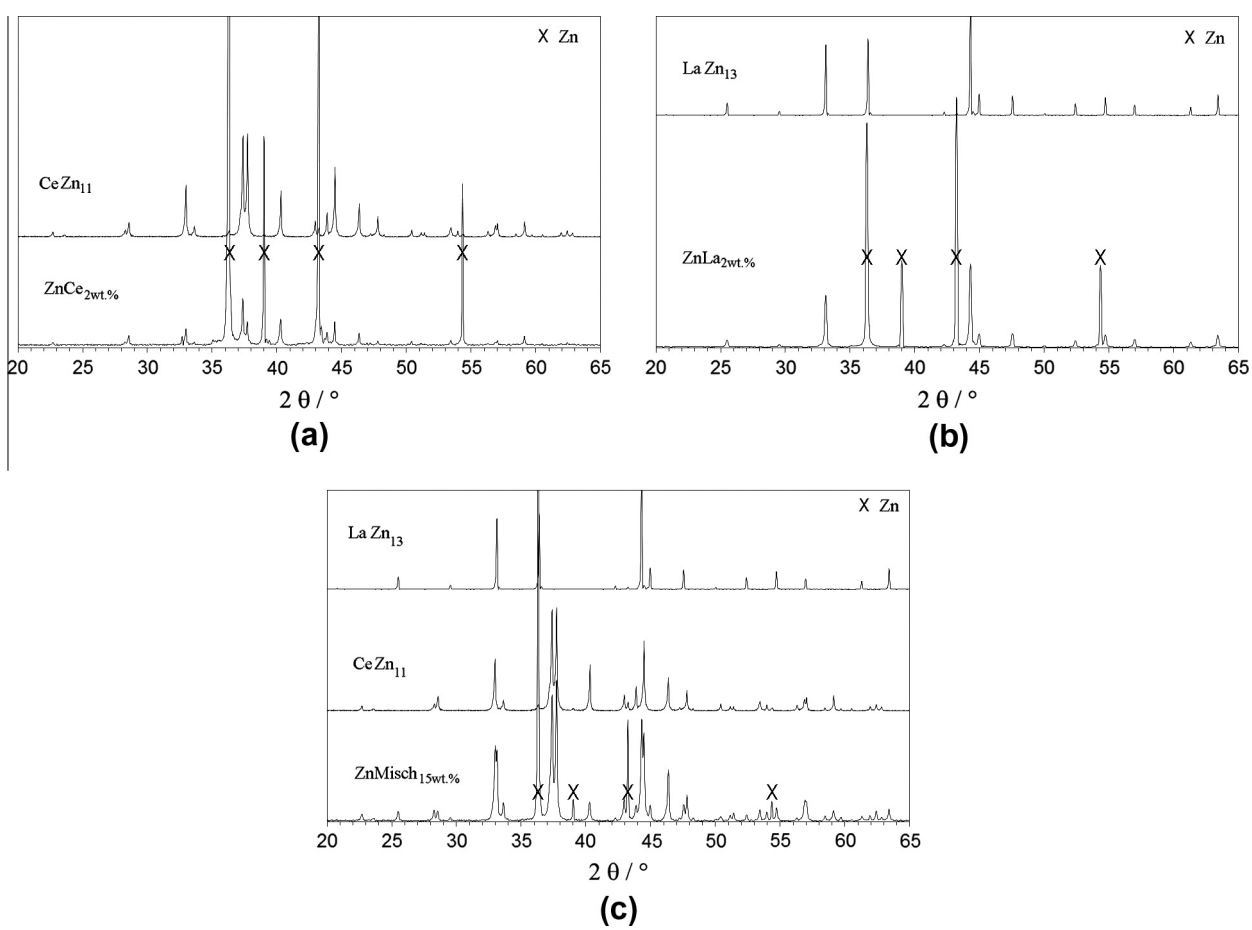

Fig. 3. X-ray diffraction patterns of ZnRE alloys and ZnRE pure intermetallic phases: RE = Ce (a); RE = La (b); RE = Mischmetal (c).

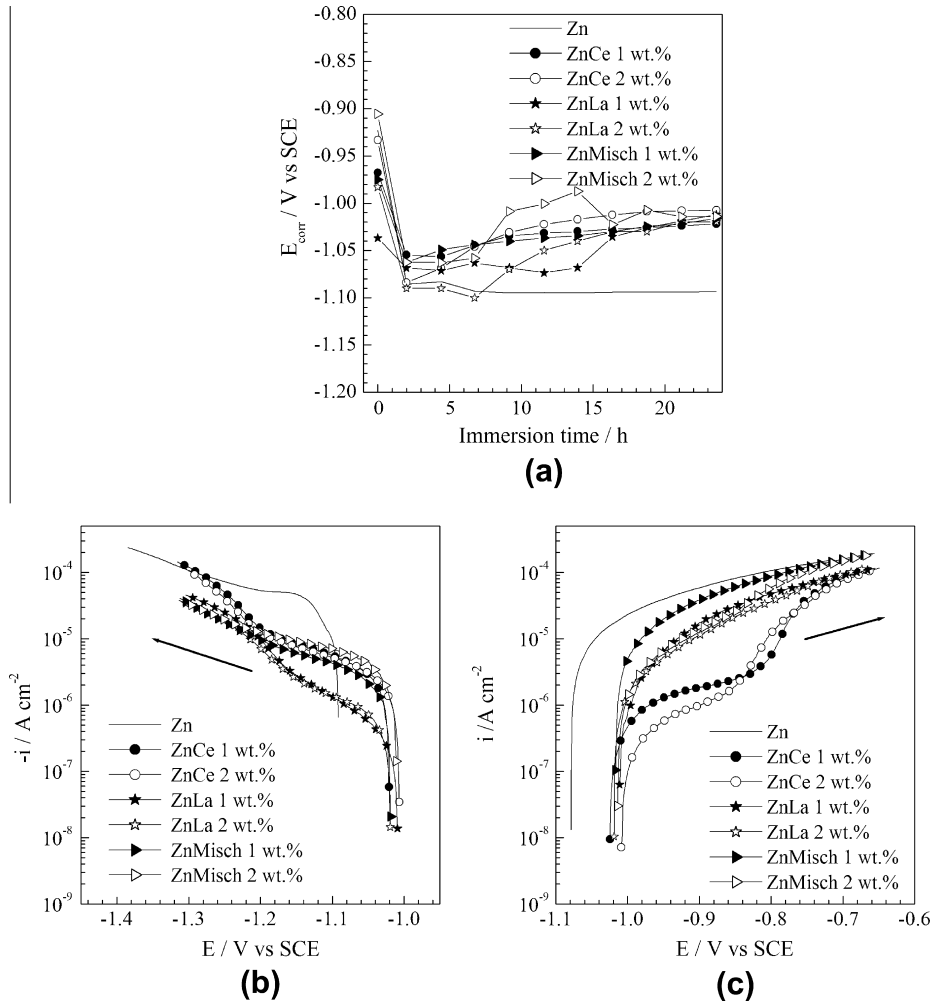

Fig. 4. Corrosion properties of ZnRE alloys compared to pure Zn in ASTM water: open-circuit potential measurements (a); cathodic (b) and anodic (c) potentiodynamic curves performed after 24 h immersion.

Finally, the three alloys can be classified regarding the anticorrosion performance and the inhibition mechanisms compared to pure zinc:

(a) The ZnCe alloys show both anodic and cathodic inhibition of corrosion phenomena compared to pure zinc.
(b) The ZnLa alloys show only a cathodic inhibition. This effect is very strong so that these alloys can be more efficient than ZnCe alloys (depending on the composition).
(c) Finally, the ZnMich alloys show the worst properties with only a slight cathodic inhibition and no inhibition of anodic processes.

3.3. Electrochemical behavior of bulk-intermetallic phases

In order to get a deeper understanding of the corrosion resistance of these alloys, the pure intermetallic phases were synthesized ($CeZn_{11}$ and $LaZn_{13}$) to be studied by electrochemistry.

As shown in Fig. 5a, the corrosion potential evolution in ASTM water is similar for both intermetallic phases, reaching a value comparable to the value observed for alloys after 24 h immersion. The two phases are nobler than pure zinc, and have a corrosion rate slightly lower than pure zinc.

The corrosion process of the intermetallic phases is obviously mainly cathodically controlled (Fig. 6b). On the cathodic region of the polarization curves, a slight inhibition of O_2 reduction can be observed in the case of $CeZn_{11}$ intermetallic phase. This phenomenon is much more significant for $LaZn_{13}$. Consequently, the corrosion rate in ASTM water of $CeZn_{11}$ is higher than the corrosion rate of $LaZn_{13}$.

The galvanic coupling measurements between each of the intermetallic phases and pure zinc were performed in ASTM water (electrode areas ratio equal to 1), and are displayed in Fig. 6. The sign of the coupling currents is consistent with the higher potential of $CeZn_{11}$ and $LaZn_{13}$ in comparison with pure zinc: both intermetallic phases are cathodic when they are electrochemically coupled with pure zinc. After a few minutes of immersion, the coupling current density of $LaZn_{13}$ is lower than for $CeZn_{11}$, which is consistent with the more significant cathodic inhibition observed previously in Fig. 5b for $LaZn_{13}$.

3.4. Surface analysis after corrosion

The corrosion products layers on ZnRE alloys were observed after 30 days of immersion in ASTM water at open-circuit potential (Fig. 7). On all the alloys, WDS measurements revealed the presence of Zn, O and C. Hydrozincite was the only crystalline phase identified by X-ray diffraction in the corrosion layers. Whereas no trace of lanthanum was detected in the corrosion layers in the case of ZnLa alloys, the chemical analysis of ZnCe corrosion layers

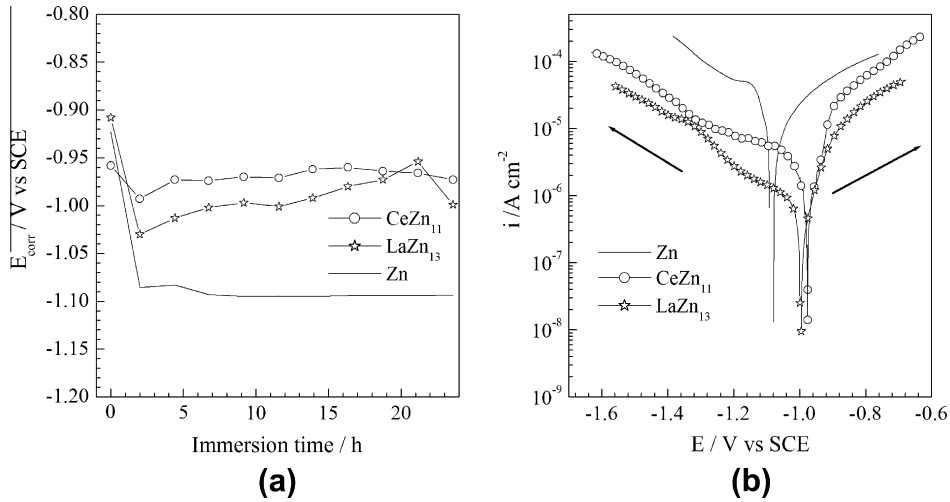

Fig. 5. Corrosion properties of $CeZn_{11}$ and $LaZn_{13}$ intermetallic phases compared to pure Zn in ASTM water: open-circuit potential measurements (a); potentiodynamic curves (b) performed after 24 h immersion.

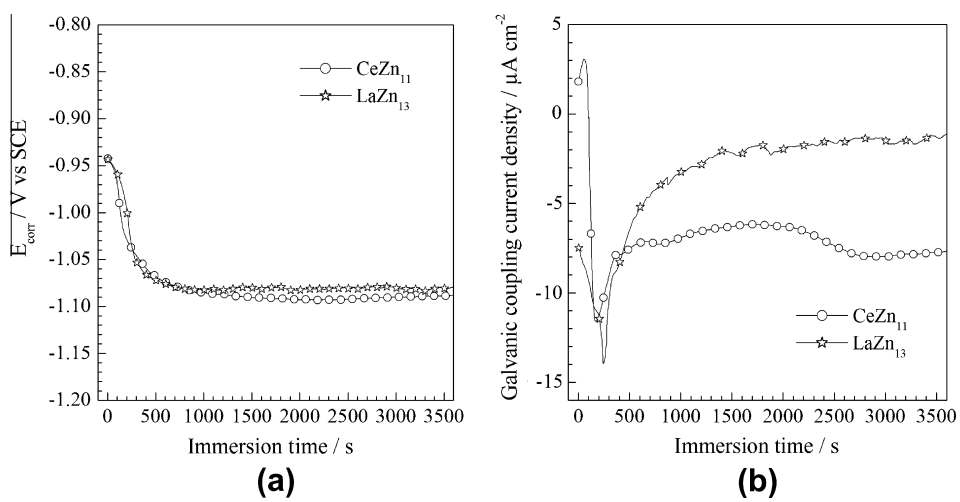

Fig. 6. Galvanic coupling in ASTM reference water between pure Zn and pure intermetallic phases ($CeZn_{11}$ and $LaZn_{13}$): coupling potential (a); galvanic coupling current density (b).

revealed the presence of cerium quite-homogeneously distributed in the corrosion layer even far from intermetallic precipitates, as proved by the X-ray map of Ce by EPMA (Fig. 7d). In the case of ZnCe 2 wt.% alloy, the concentration of cerium in the corrosion layer could be evaluated to 0.1 wt.%.

As already observed for ZnCe alloys [10] and consistently with electrochemical coupling results, $LaZn_{13}$ intermetallic precipitates (white particles in Fig. 7a) act mainly as cathodic site, so that the oxidation preferentially affects the zinc matrix. The $LaZn_{13}$ and $CeZn_{11}$ phases are slightly oxidized as shown on the Fig. 7a in the case of ZnLa 2 wt.% alloy.

Concerning the ZnMish alloys, contrary to $LaZn_{13}$ and $CeZn_{11}$ intermetallic phases, the two ternary intermetallic phases are oxidized by the solution at the same time as the zinc matrix. The resulting corroded products, flaky-shaped, are constituted of cerium, lanthanum and a large amount of oxygen as revealed by EDS point analyses performed on cross sections. They are inserted in the corrosion layer, as displayed on the Fig. 7b. So, in the case of ternary alloys, the intermetallic phases are oxidized, but the lanthanum and cerium element are not homogenously dispersed in the corrosion layer.

4. Discussion

From the overall electrochemical results, rare-earth addition to zinc metal reduces the corrosion rate of the alloys by inhibiting both the cathodic reaction of oxygen reduction, and the anodic reaction of zinc oxidation. This improvement of the anticorrosion performance by rare earth addition is comparable to the decrease of the corrosion rate brought by the addition of rare-earth salts in the corrosive medium or in a protective layer, described in some studies relative to zinc [24,25] to aluminum [26] or Al–Zn–In alloys [27].

In the case of ZnRE alloys, the electrochemical effect of cerium and lanthanum is closely linked to the microstructure of the alloy, especially the composition and distribution of the intermetallic phases: $CeZn_{11}$ and $LaZn_{13}$ for binary alloys or $Ce_{1-x}La_xZn_{11}$ and $Ce_yLa_{1-y}Zn_{13}$ for ternary alloys. Indeed, despite the low amount of rare-earth in the alloy, the bulk concentration in RE-enriched intermetallic precipitates is important (as displayed in the Fig. 3) because the rare-earth content in the intermetallic phases is low.

Three phenomena have to be considered to get a comprehensive understanding of the corrosion behavior of the alloys: the

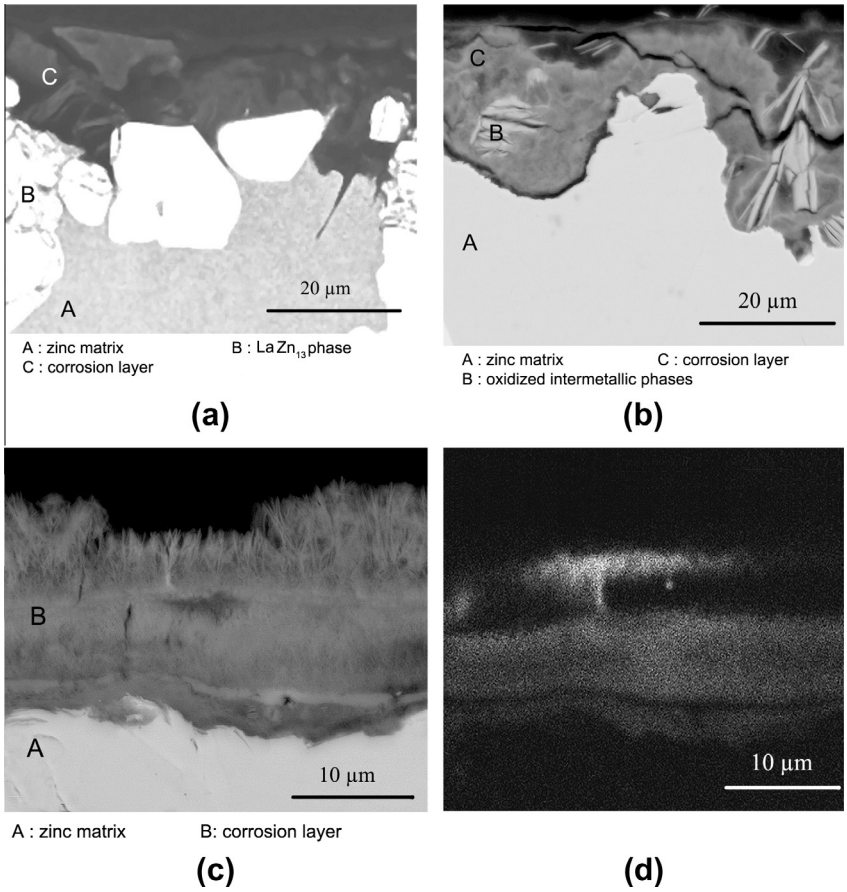

Fig. 7. Cross-section corrosion layers observed on ZnRE alloys immersed 30 days in ASTM water: ZnLa 2 wt.% (a), ZnMisch 2 wt.% (b), ZnCe 2 wt.% far from intermetallic particules: BSE image (c) and corresponding EPMA X ray-map of Ce (d).

intrinsic corrosion of pure zinc, the intrinsic corrosion of the intermetallic phases and the galvanic coupling between zinc matrix and the precipitated intermetallic ZnRE phases. From an electrochemical point of view, anodic and cathodic currents I_a and I_c can be described respectively by equations 1 and 2:

$$I_a = i_{a,Zn} \cdot S_{Zn} + i_{a,IM} \cdot S_{IM} \quad (1)$$

$$I_c = i_{c,Zn} \cdot S_{Zn} + i_{c,IM} \cdot S_{IM} \quad (2)$$

where $i_{a,Zn}$ and $i_{c,Zn}$ are respectively the anodic and cathodic current densities on the zinc matrix; $i_{a,IM}$ and $i_{c,IM}$ are respectively the anodic and cathodic current densities on the intermetallic phases; S_{Zn} and S_{IM} are respectively the zinc matrix area and the intermetallic phases area in contact with the electrolyte.

The corrosion point of the alloys is defined by $I_a = I_c$. In many cases, the galvanic coupling is the determining factor, with a high corrosion potential difference between the matrix and the nobler intermetallic phases. Therefore, at the corrosion potential, the contribution of the intermetallic phases to the anodic current is negligible as well as the contribution of the zinc matrix to the cathodic current. In these cases, the oxidation and reduction reactions inducing the corrosion are decoupled: the oxygen reduction is localized at the surface of the precipitates whereas the oxidation affects the zinc matrix.

However, in the specific case of the ZnRE alloys, the corrosion potential difference between the zinc matrix and the zinc rich intermetallic phases is rather low (less than 100 mV). Moreover, the values of the corrosion current densities of the intermetallic phases are in the same order of magnitude as the values of galvanic coupling current densities (around 1 $\mu A\,cm^{-2}$). Therefore, even if the area covered by the intermetallic phases is around 20% of the total area in contact with the electrolyte, the oxidation of the intermetallic phases cannot be neglected in the general corrosion process of the alloys.

This oxidation of the intermetallic phases explains the anodic inhibition observed especially on ZnCe alloys, with the apparition of a passivation plateau. Actually, a study by electrochemical impedance spectroscopy described in a precedent work [10] has shown a modification of the dielectric properties of the passive layer grown at the alloys surface. In parallel, the homogeneous presence of cerium in the corrosion layer (in very low quantity) even far from the intermetallic precipitates could be highlighted by X-ray cartography in this work. The passivating properties of the corrosion layer are thus reinforced by the presence of a zinc/cerium mixed compound, inducing the decrease of the anodic reaction rate. This phenomenon has already been observed for ZnAl alloys for example [7]: at their surface, a double (Zn^{2+}, Al^{3+}) lamellar hydroxide compounds increases the density, the adhesion and therefore the protective properties of the layer of corrosion products. In the specific case of ZnLa alloys, the anodic inhibition is slight and at the same time no lanthanum was detected in the corrosion layer by EPMA analysis after 1 month immersion. However, this slight anodic inhibition could be explained by the presence of a very low quantity (below the detection limit 600 ppm), because lanthanum salt can be efficient at a very low level as revealed by some corrosion inhibition studies [28].

Concerning the cathodic inhibition observed on the alloys, the galvanic coupling is the key parameter. The cathodic inhibition observed on ZnRE alloys is mainly due to the cathodic inhibition observed on the ZnRE intermetallic phases. This phenomenon is

actually more significant for ZnLa alloys than for ZnCe alloys since the cathodic inhibition for the $Zn_{13}La$ pure intermetallic phase is more significant than for the $Zn_{11}Ce$ pure intermetallic phase.

In the case of ZnMisch alloys (up to 2 wt.%), the electrochemical behavior of alloys only shows a slight inhibition of cathodic reaction of corrosion process. No inhibition of anodic reaction of alloys was observed by the addition of Mischmetal (75/25 wt.% of Ce/La). Globally, the alloys seem to contain not enough lanthanum to induce a strong cathodic inhibition, comparable to ZnLa alloys, and not enough cerium to produce an efficient anodic inhibition, comparable to ZnCe alloys. This effect can be due to the particular behavior of ternary intermetallic phases. Indeed, the metallographic observations have shown that the ternary phases are rapidly oxidized and entirely incorporated to the corrosion layer. Further studies on the pure ternary intermetallic phases could be useful to more completely characterize the electrochemical behavior of ternary ZnLaCe alloys.

5. Conclusion

Low amounts of cerium or lanthanum added to zinc induce an improvement of its corrosion resistance. In these alloys, the two rare-earth metals are homogeneously dispersed through the precipitation in the zinc matrix of two intermetallic compounds: $CeZn_{11}$ and $LaZn_{13}$, consistently to the binary phase diagrams. In the case of ZnCeLa alloys (synthesized from mischmetal composition), new ternary intermetallic compounds were characterized, $Ce_{1-x}La_xZn_{11}$ and $Ce_yLa_{1-y}Zn_{13}$, and their equilibrium with zinc matrix was confirmed by phase diagram calculation.

The electrochemical effect of rare-earth addition is closely related to electrochemical behavior of intermetallic phases in the alloys. $CeZn_{11}$ and $LaZn_{13}$ induce a cathodic inhibition of the oxygen reduction in comparison with pure zinc. For Zn–Ce alloys, the electrochemical corrosion rate of $CeZn_{11}$ phase is sufficient to allow the Ce^{3+} release and the formation of a Ce enriched passive layer, leading to a further anodic inhibition of the corrosion processes. Concerning the Zn–Mischmetal alloys, the low content of lanthanum and cerium in the observed ternary intermetallic phases does not allow bringing particular benefits for the corrosion resistance of the zinc matrix.

Acknowledgements

This study was performed in the framework of a Franco-Algerian research project (Tassili No. 09MDU762).

References

[1] X.G. Zhang, Corrosion and Electrochemistry of Zinc, Plenum Press, New York, 1996.
[2] S.W.K. Morgan, Zinc and its Alloys and Compounds, John Wiley and Sons, Toronto, 1985.
[3] F. Zhu, D. Persson, D. Thierry, Formation of corrosion products on open and confined metal surfaces exposed to periodic wet/dry conditions – a comparison between zinc and electrogalvanized steel, Corrosion 57 (2001) 582–590.
[4] F. Zhu, D. Persson, D. Thierry, C. Taxen, Formation of corrosion products on open and confined zinc surfaces exposed to periodic wet/dry conditions, Corrosion 56 (2000) 1256–1265.
[5] E. Ivaskevic, A. Sekskis, A. Kalinicenko, R. Ramanauskas, Selective dissolution of electrodeposited ZnNi alloy coating, Trans. Inst. Metal Finish. 82 (2004) 93–97.
[6] K.R. Baldwin, M.J. Robinson, C.J.E. Smith, Corrosion rate measurements of electrodeposited Zinc–Nickel alloy coatings, Corros. Sci. 36 (1994) 1115–1131.
[7] Y. Li, Formation of nano-crystalline corrosion products on Zn–Al alloy coating exposed to seawater, Corros. Sci. 43 (2001) 1793–1800.
[8] F. Rosalbino, E. Angelini, D. Maccio, A. Saccone, S. Delfino, Influence of rare-earths addition on the corrosion behaviour of Zn–5%Al (Galfan) alloy in neutral aerated sodium sulphate solution, Electrochim. Acta 52 (2007) 7107–7114.
[9] F. Rosalbino, E. Angelini, D. Maccio, A. Saccone, S. Delfino, Application of EIS to assess the effect of rare-earths small addition on the corrosion behaviour of Zn–5%Al (Galfan) alloy in neutral aerated sodium chloride solution, Electrochim. Acta 54 (2009) 1204–1209.
[10] K. Guessoum, D. Veys-Renaux, E. Rocca, K. Belhamel, Corrosion behaviour of zinc–cerium alloys: role of intermetallic phases, Corros. Sci. 53 (2011) 1639–1645.
[11] J. Elvins, J.A. Spittle, D.A. Worsley, Microstructural changes in zinc aluminium alloy galvanising as a function of processing parameters and their influence on corrosion, Corros. Sci. 47 (2005) 2740–2759.
[12] N.C. Hosking, M.A. Ström, P.H. Shipway, C.D. Rudd, Corrosion resistance of zinc-magnesium coated steel, Corros. Sci. 49 (2007) 3669–3695.
[13] A.E. Ares, L.M. Gassa, Corrosion susceptibility of Zn–Al alloys with different grains and dendritic microstructures in NaCl solutions, Corros. Sci. 59 (2012) 290–306.
[14] C.P. Wang, X. Chen, X.J. Liu, F.S. Pan, K. Ishida, Thermodynamic modelling of Ce–Zn and Pr–Zn systems, J. Alloy. Compd. 458 (2008) 166–173.
[15] H.Y. Qi, G.X. Huang, R.D. Liu, K. Zhang, L.B. Liu, Z.P. Jin, Thermodynamic optimization of La–Zn and La–Mg–Zn systems, J. Alloy. Compd. 497 (2010) 336–343.
[16] L. Kaufman, H. Bernstein, Computer Calculation of Phase Diagrams, Academic Press, New York, 1970.
[17] C. Guo, Z. Du, C. Li, A thermodynamic description of Ce–La–Mg system, Int. J. Mater. Res. 101 (2012) 1424–1431.
[18] K.A. Gschneidner, F.W. Calderwood, The Ce–La (Cerium–Lanthanum) system, Bull. Alloy Phase Diagrams 2 (1982) 445–447.
[19] SGTE Solution Database, Version 2004, provided by Thermo-Calc Software AB, Stockholm, Sweden <www.thermocalc.se>.
[20] Annual book of ASTM standards, Copyright ASTM, PA, 1986.
[21] A.A. Rahim, E. Rocca, J. Steinmetz, M.J. Kassim, Inhibitive action of mangrove tannins and phosphoric acid on pre-rusted steel via electrochemical methods, Corros. Sci. 50 (2008) 1546–1550.
[22] A. Mesbah, C. Juers, F. Lacouture, S. Mathieu, E. Rocca, M. François, J. Steinmetz, Inhibitors for magnesium corrosion: metal organic frameworks, Solid State Sci. 9 (2007) 322–328.
[23] C. Georges, E. Rocca, P. Steinmetz, Synergistic effect of tolutriazol and sodium carboxylates on zinc corrosion in atmospheric conditions, Electrochim. Acta 53 (2008) 4389–4845.
[24] K. Aramaki, Synergistic inhibition of zinc corrosion in 0.5 M NaCl by combination of cerium(III) chloride and sodium silicate, Corros. Sci. 44 (2002) 871–886.
[25] M.F. Montemor, A.M. Simões, M.G.S. Ferreira, Composition and corrosion behaviour of galvanised steel treated with rare-earth salts: the effect of the cation, Prog. Org. Coat. 44 (2002) 111–120.
[26] E.A. Matter, S. Kozhukharov, M. Machkova, V. Kozhukharov, Comparison between the inhibition efficiencies of Ce(III) and Ce(IV) ammonium nitrates against corrosion of AA2024 aluminum alloy in solutions of low chloride concentration, Corros. Sci. 62 (2012) 22–33.
[27] W. Xiong, G.T. Qi, X.P. Guo, Z.L. Lu, Anodic dissolution of Al sacrificial anodes in NaCl solution containing Ce, Corros. Sci. 53 (2011) 1298–1303.
[28] K. Aramaki, The inhibition effects of cation inhibitors on corrosion of zinc in aerated 0.5 M NaCl, Corros. Sci. 43 (8) (2001) 1573–1588.